Ab initio curved-wave x-ray-absorption fine structure

J. Mustre de Leon,* J. J. Rehr, and S. I. Zabinsky
Department of Physics, FM-15, University of Washington, Seattle, Washington 98195

R. C. Albers
Theoretical Division, Los Alamos National Laboratory, Los Alamos, New Mexico 87545
(Received 25 April 1991)

The most important elements of *ab initio* calculations of x-ray-absorption fine structure (XAFS) are studied. To obtain accurate results without *ad hoc* adjustable parameters, we find it essential to include (i) curved-wave effects, (ii) a complex, energy-dependent self-energy, (iii) an approximate molecular potential, and (iv) a fixed energy reference for the photoelectron wave number. Based on these findings, an automated code has been developed for *ab initio* calculations of single-scattering XAFS, in which curved-wave effects are treated exactly in terms of effective backscattering amplitudes, inelastic losses and self-energy shifts are incorporated with use of a Hedin-Lundqvist self-enegy, an automated relativistic overlapping-atom muffin-tin potential is used, and the energy threshold is estimated from electron-gas theory. The efficiency of the code is made possible by analytic expressions for the Hedin-Lundqvist self-energy. This code replaces existing tables of XAFS phases and scattering amplitudes and yields reliable theoretical XAFS standards for arbitrary pairs of atoms throughout the Periodic Table ($Z \leq 94$). These results are comparable to those from self-consistent calculations and are valid to within about 20 eV of the absorption edge. Comparisons with experiment are presented for Cu, Ge, Pt, Br_2, and $GeCl_4$. The calculated XAFS amplitudes are found to be accurate to within 15%; XAFS phases are accurate to within 0.2 rad; and nearest-neighbor distances are typically accurate to within 0.02 Å.

I. INTRODUCTION

X-ray-absorption fine structure (XAFS), i.e., the oscillatory structure in the x-ray-absorption coefficient, contains much quantitative information about the local atomic structure surrounding an absorbing atom. This information includes near-neighbor distances R, coordination numbers N_R, and structural and vibrational disorder in bond distances σ^2, i.e., the structural quantities appearing in the curved-wave XAFS equation,

$$\chi_l(E) = -\sum_R N_R S_0^2 \frac{|f_{\rm eff}(\pi,k,R)|}{kR^2} \times \sin(2kR + 2\delta^c + \Phi_{\rm eff}) e^{-2\sigma^2 k^2} e^{-2R/\lambda} . \quad (1)$$

Here, $f_{\rm eff}(\pi,k,R) = |f_{\rm eff}(\pi,k,R)| e^{i\Phi_{\rm eff}}$ is the effective curved-wave backscattering amplitude,[1] δ^c is the final-state l-wave central-atom phase shift, λ is the mean free path of the photoelectron, and S_0^2 is a many-body amplitude reduction factor, all of which must be taken into account to extract structural information from experiment. Thus XAFS analysis always requires a comparison with an accurately known reference system, either experimental or theoretical.

Heretofore, theoretical standards have usually been less successful than experimental standards because of the approximations and *ad hoc* parameters needed in theoretical models.[2,3] Tables of extended x-ray-absorption fine structure (EXAFS) phases and amplitudes are the most commonly used theoretical standards,[3,4] and each of the previously available tabulations has its drawbacks: The tables of Teo and Lee[3] are based on a theory appropriate to the EXAFS regime, which takes into account inelastic losses and self-energy shifts but neglects curved-wave effects. The tables of McKale *et al.*[4] take curved-wave effects into account but neglect inelastic losses. Both of these tabulations require the use of the energy reference or "inner potential" E_0 as a free fitting parameter. Since such *ad hoc* parameters compensate for other errors in the theory, such as those caused by the plane-wave approximation (PWA) or errors in the scattering potential, they need not have a direct physical interpretation. Our goal in this work is to develop a more complete theoretical model, which remedies the above drawbacks and reduces as much as possible the need for such fitting parameters.

There are several key factors in the theory. The importance of curved-wave corrections in XAFS has been addressed by several authors.[1,5–10] It is found that the PWA introduces errors of up to 1 rad in the XAFS phase and up to 25% in the amplitude, even at energies above 70 eV from the edge.[5] Moreover, the high-energy regime appropriate to EXAFS is not the PWA, but rather an asymptotic theory that includes important spherical-wave corrections.[1] As curved-wave corrections are now well understood, we focus our attention on the other important ingredients in the theory. The need in XAFS calculations for scattering potentials, which include a complex, energy-dependent self-energy, has also been discussed.[2,8,11,12] Ground-state potentials can introduce errors of 0.1 Å in nearest-neighbor distance determinations.[2] These phase errors remain even if inelastic losses are included phenomenologically, in terms of a mean free

path. Such errors can be partially corrected with a shift in E_0, but only at high energies. The construction of the scattering potential is another important consideration, and approximations such as nonrelativistic- or renormalized-atom potentials have limited validity. Finally, a consistent energy reference E_0 when comparing theory and experiment is important to render physical significance to shifts in E_0. One of the main goals of this work is to assess the relative importance of these factors in a quantitative theory of XAFS. We do *not* discuss multiple-scattering corrections in this paper; however, we may expect that the same considerations for the scattering potential and self-energy will apply in more complete applications that include multiple scattering.

The remainder of this paper is outlined as follows. In Sec. II we describe each step in the calculation of XAFS spectra. Section III details different prescriptions for the scattering potential and their effects on XAFS phases and amplitudes. Section IV contains a brief discussion of our *ab initio* code FEFF based on the results of III. Section V contains several comparisons with experiment, and Sec. VI contains a summary and conclusions. A brief description of FEFF, which focuses on the results for the new XAFS phases and amplitudes, rather than the underlying theory, will be published elsewhere.[13]

II. *Ab initio* XAFS CALCULATIONS

In this section the basic steps in the calculation of XAFS are described.

A. Atomic charge densities

The importance of relativistic calculations of atomic charge densities in the generation of XAFS scattering potentials has been stressed by Teo and Lee,[3] especially for heavy atoms. They find, for W, for example, that nonrelativistic charge densities lead to errors as big as 0.8 rad in the EXAFS phase and 10% in the amplitude, at energies as high as $k=5$ Å^{-1}. Such errors are comparable to those caused by the PWA. Consequently, we use a self-consistent Dirac-Fock-Slater atom code. Our atom code is adapted from the Hartree-Fock program of Desclaux.[14] We have automated the code to calculate charge densities for any atom in the Periodic Table up to americium, with a single input parameter, the atomic number Z. In the case of the absorbing atom, the atomic configuration is chosen as that with a hole in a given core-hole state (K, $L_{\rm I}$, etc.) and an extra electron in the first unoccupied level of its electron configuration. This corresponds to the electronic configuration of a neutral (i.e., screened) atom of atomic number $Z+1$ with a core hole and local atomic screening. Screening of electrons in neighboring atoms is ignored. This is an approximation to a fully relaxed final state. By comparison, Lee and Beni[2] and Teo and Lee[3] approximate the absorbing atom with $(Z+1)$-atom charge densities. We feel that our prescription is an improvement, since it is based on self-consistent calculations and since the XAFS is dominated by the fully relaxed primary channel.[8]

The starting point of the charge-density calculation is the self-consistent solution of the Dirac equation for all occupied electron states in the spherical potential, $V_{\rm at}(r)=V_C(r)+V_{\rm xc}(\rho_{\rm at}(r))$. Here $V_C(r)$ includes the Coulomb potential of the nucleus and the Hartree potential, and $V_{\rm xc}(\rho)$ is the von Barth–Hedin local-density approximation to the exchange-correlation potential.[15–17] The spherically averaged atomic charge density is calculated from the radial parts of the spinor components for each electron in the atom, summed over all occupied states.

B. Ground-state muffin-tin potential

Given the atomic charge densities and atomic potentials, we construct the scattering muffin-tin potential following one of several prescriptions, including renormalized-atom potentials, overlapped-atom potentials, and self-consistent potentials. Details are discussed in Sec. III below. We find that an overlapped-atom potential yields XAFS phases and amplitudes comparable to those from self-consistent molecular potentials.[18,19] The renormalized atom is found to be unreliable in polyatomic materials. In addition to the ground-state muffin-tin potential, $V(r)=V_C(r)+V_{\rm xc}(\rho(r))$, a muffin-tin charge density $\rho(r)$, and interstitial potentials $V_{\rm int}$ and charge densities $\rho_{\rm int}$ are generated.

C. Electron self-energy

To obtain excited-state wave functions, the Schrödinger equation must be replaced by a Dyson equation in which the role of the ground-state exchange-correlation potential $V_{\rm xc}$ is taken by the electron self-energy $\Sigma(E,\rho)$.[2] Our self-energy, which is intended for energetic photoelectrons, is constructed within the local density approximation,[15] using the ground-state local charge density. Because the self-energy is not as well understood as ground-state $V_{\rm xc}$, we have considered several commonly used forms. Besides the complex-energy-dependent Hedin-Lundqvist (HL) self-energy,[20,21] one may use the real-valued, energy-dependent Dirac-Hara (DH) potential,[22] or energy-independent ground-state $V_{\rm xc}$,[16] together with a constant imaginary part. In our formulation we define the excited-state self-energy such that it reduces to the ground-state $V_{\rm xc}(\rho)$ at threshold $E=\mu$. For the HL potential, for example,

$$\Sigma(E,\rho)=\Sigma_{\rm HL}(E,\rho)-\Sigma_{\rm HL}(\mu,\rho)+V_{\rm xc}(\rho)\ . \tag{2}$$

D. Energy reference E_0

As an approximation to the energy threshold, we identify the energy reference E_0 with the chemical potential of a homogeneous electron gas at the interstitial density with density parameter r_s,

$$\mu=\tfrac{1}{2}k_F^2(r_s)+V_{\rm int}(\mu,\rho_{\rm int})\ , \tag{3}$$

where $k_F(r_s)=1.9192/r_s$ is the local Fermi momentum, $r_s=(3/4\pi\rho_{\rm int})^{1/3}$, and $V_{\rm int}(\mu,\rho)$ is the interstitial potential at threshold. This approximation introduces tolerable errors of a few eV in the estimated chemical potential com-

pared with self-consistent calculations, the latter yielding a slightly lower value. In the case of Cu, $\mu - V_{\rm int}$ differs by about 4 eV from the result of self-consistent band-structure calculations.[19,23]

When comparing with experiment it should be noted that the value of the chemical potential μ depends on the density of states near the threshold and generally does not correspond to the midpoint of the absorption edge. Thus it is desirable to fix the experimental energy reference by matching the peaks observed in measurements of the total x-ray-absorption curve $\mu(E)$ to near edge calculations.

E. Partial-wave phase shifts

The calculation of XAFS requires the solution of a scattering problem in which the excited photoelectron moves freely in a background interstitial potential $V_{\rm int}(E)$ and is scattered by muffin-tin potentials,

$$\Delta V(E,r) = V(E,r) - V_{\rm int}(E) ,$$

that vanish outside the muffin-tin radii. Thus we determine complex partial-wave phase shifts for every atom by integrating the Dirac equation (neglecting the spin-orbit coupling) up to the muffin-tin radius with the scattering potential $\Delta V(E,r)$ and matching to decaying free spherical waves with wave vector

$$p = \sqrt{2[E + i\Gamma/2 - V_{\rm int}(E)]} .$$

We determine $l_{\rm max}(p)$ phase shifts at each energy, where $l_{\rm max} \sim pR_{\rm MT}$, i.e., up to about 20 phase shifts for $k \leq 20$ Å^{-1}.

F. Curved-wave XAFS calculation

We determine the exact, curved-wave, single-scattering XAFS spectrum, $\chi_l(E)$ from[1]

$$\chi_l(E) = -\mathrm{Im} \sum_R N_R S_0^2 \frac{\tilde{f}(\pi,p,R)}{pR^2} e^{i(2pR + 2\delta^c)} e^{-2\sigma^2 p^2} . \quad (4)$$

In Eq. (4) it is assumed that only a single final-state angular momentum, $l = l_f$, is important, which is generally a good approximation.[24] Thus for $L_{\rm II}$ or $L_{\rm III}$ absorption we only include transitions to a d final state. For K-shell absorption in a polycrystalline sample, for example, the effective scattering amplitude

$$\tilde{f}(\pi,p,R) = |\tilde{f}(\pi,p,R)| e^{i\tilde{\Phi}}$$

is

$$\tilde{f}(\pi,p,R) = \frac{1}{p} \sum_l (-1)^l (2l+1) \times t_l \left[\frac{(l+1)c_{l+1}^2(pR) + l c_{l-1}^2(pR)}{2l+1} \right] . \quad (5)$$

Here $c_l(x) = i^l x e^{-ix} h_l(x)$ is the polynomial part of the spherical Hankel functions, which is calculated exactly by recursion. For *polarized* x rays we still can use Eq. (4),[25,26] for K-shell absorption in a single crystal, provided we replace $\tilde{f}(\pi,p,R)$ by

$$\tilde{f}(\pi,p,R,\theta_R) = \cos^2\theta_R \, \tilde{f}^{(0)}(\pi,p,R) + \sin^2\theta_R \, \tilde{f}^{(1)}(\pi,p,R) , \quad (6)$$

where θ_R is the angle between the bond vector **R** and the polarization vector ϵ, and

$$\tilde{f}^{(0)}(\pi,p,R) = \frac{1}{p} \sum_l (2l+1)(-1)^l \times t_l \frac{[(l+1)c_{l+1}(pR) + l c_{l-1}(pR)]^2}{(2l+1)^2} , \quad (7a)$$

$$\tilde{f}^{(1)}(\pi,p,R) = -\frac{1}{p} \sum_l (2l+1)(-1)^l t_l \frac{l(l+1)}{2} \frac{c_l^2(pR)}{(pR)^2} . \quad (7b)$$

Expressions for absorption from an arbitrary shell have been given by Benfatto *et al.*[27] We remark that although Eq. (1) and Eq. (4) give the same results for χ_l, the quantities appearing in these equations are *not* the same, since the complex photoelectron momentum p, which is referenced to $V_{\rm int}$, is not the same as the wave number k, which is referenced to threshold.

It is essential that the extrinsic loss of the photoelectron be adequately taken into account. These losses can be assigned to three physical processes: (i) inelastic scattering by a uniform electron gas of density equal to the average interstitial density, which is represented by $\exp(-2R\,\mathrm{Im}p)$, i.e., by a mean free path for the photoelectron $\lambda = 1/\mathrm{Im}p$, (ii) inelastic scattering in backscattering atoms contained in $\tilde{f}(\pi,p,R)$, and (iii) inelastic scattering within the absorbing atom given by $\exp(-\mathrm{Im}2\delta^c)$. Since the imaginary part of the scattering muffin-tin potential, $\mathrm{Im}[\Sigma(E,\rho(r)) - \Sigma(E,\rho_{\rm int}]$, is positive deep within an atom where $\mathrm{Im}\Sigma(E,\rho)$ vanishes (see Fig. 1), terms (ii) and (iii) can also contain inelastic gains.

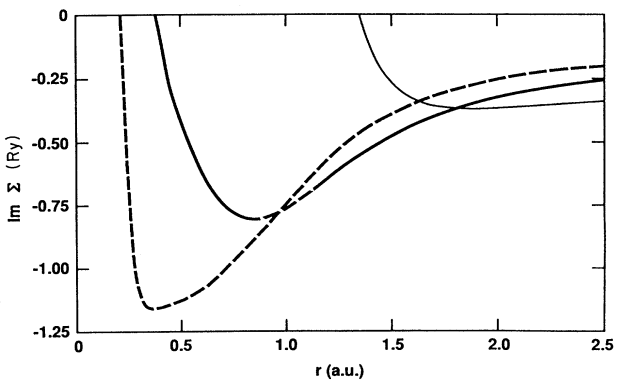

FIG. 1. Imaginary part of the Hedin-Lundqvist self-energy for photoelectrons with $E = 64$ Ry (dashed line), $E = 25$ Ry (thick solid line), and $E = 1$ Ry (thin solid line), in a Cu atom.

However, the inclusion of all three terms prevents double counting of inelastic losses.

We note that the definition of

$$p=\sqrt{2[E+i\Gamma/2-V_{\rm int}(E)]}$$

and the fact that $V_{\rm int}(E)$ is energy dependent implies that our definition of the XAFS phase is different from other formulations where the vacuum or another fixed energy is taken as the energy reference. The effect of a real energy reference, as in Refs. 2 and 3, on the backscattering amplitude and phase was discussed by Tran Thoai and Ekardt in the context of plane-wave calculations.[28] They observed differences in the phase of up to 1 rad and differences in amplitude of up to 20%.[29]

Other inelastic losses must also be considered. Inelastic processes related to the relaxation of the core hole give rise to the many-electron overlap reduction factor S_0^2 and a core-hole lifetime broadening, i.e., $E\rightarrow E+i(\Gamma/2)$. This broadening also gives a contribution to the mean free path discussed above. In our program default values for Γ are interpolated from the tables in Ref. 30. Values for S_0^2 are taken from independent calculations or experimental measurements.[8,31,32] Typical values are $S_0^2\cong 0.85-1.1$. This simple prescription seems to remain a reasonable approximation even when interference between intrinsic and extrinsic losses is included.[12] However, a more complete treatment of the energy dependence of S_0^2 is desirable,[8] and its use as a constant fitting parameter is one of the least satisfactory aspects of our present work.

III. SCATTERING POTENTIAL IN XAFS

Motivated by the need to understand what constitutes an adequate treatment of the scattering potential in EXAFS, we have compared several different prescriptions. In this section we study their effect on calculated XAFS amplitudes and phases. First we discuss prescriptions for the Coulomb potential V_C and second prescriptions for the self-energy $\Sigma(E,\rho)$. We also present a new explanation for the energy scaling that was observed to give agreement between experiment and band-structure calculations of x-ray absorption.

A. Coulomb potential

Although chemical effects may be well approximated by self-consistent calculations of the potential,[18,19] it is as yet impractical to carry out such calculations routinely. Thus the accuracy of less precise approximations must be assessed. To this end we considered the following prescriptions for the Coulomb contribution to the scattering potential: free-atom potentials, "renormalized-atom" potentials, overlapped-atom potentials, and a self-consistent potential obtained from band-structure calculations. For the moment the self-energy will be ignored. The total ground-state scattering potential is then calculated by adding to the Coulomb contribution $V_C(\mathbf{r})$, the ground-state exchange-correlation potential, of von Barth and Hedin.[17]

All the XAFS calculations were performed following the outline in Sec. II. For calculations using free-atom potentials, phase shifts were computed with the scattering potential set to zero outside the Wigner-Seitz sphere. The renormalized-atom potential was generated by truncating the charge density outside the Wigner-Seitz radius, $r_{\rm WS}$ and reintroducing it inside as a constant charge density. The contributions V_C and $V_{\rm xc}$ were then calculated from this renormalized-charge density. The interstitial potential and charge density were taken to be the values at the Wigner-Seitz radius. The overlapped-atom potential is constructed according to the Mattheiss prescription:[33] In this method atomic charge densities are overlapped and spherically symmetrized around each site. In our approach the muffin-tin radii around each atom are chosen according to the Norman prescription,[34] in which the charge around each atom of atomic number Z is integrated up to the Norman radius r_N defined as the radius of a neutral sphere containing Z electrons. This is analogous to the unit-cell charge neutrality requirement in the Wigner-Seitz method. The muffin-tin radii are then obtained by scaling the r_N by a constant factor until the muffin-tins touch. Overlapping by 10% does not significantly change the XAFS, so we do not consider this effect here. The interstitial averages are determined by averaging the charge and potential between the muffin-tin and Norman radii.[35] While the renormalized-atom method gives results for monatomic materials comparable in accuracy to those based on the Mattheiss prescription (see Fig. 2), its use in polyatomic materials ignores chemical bonding effects and leads to unacceptable discontinuities in muffin-tin zeros.[29,34] For this reason an overlapped-atom potential is generally preferable. Finally, to assess the importance of self-consistency, we used a self-consistent potential obtained from linear muffin-tin orbital band-structure calculations.[19]

In Fig. 2 we compare the phase of filtered $k^2\chi$ XAFS from Cu experiment[32] at 190 K and from calculations with $R=2.540$ Å using the above prescriptions. We also

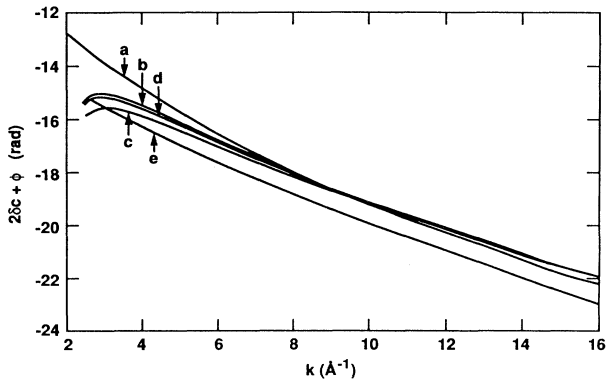

FIG. 2. Filtered XAFS phase ($2\delta^c+\Phi$) for the first coordination shell of Cu (K edge) with ground-state potentials: (a) tables of Ref. 4, (b) atomic potential, (c) self-consistent potential, (d) "renormalized-charge" potential (indistinguishable from overlapped potential curve), and (e) experimental data.

present a curve based on the tables of Ref. 4. Since the ground state V_{xc} was used in this comparison, no extrinsic losses were included, and all calculated amplitudes were larger than the experimental amplitude. In the phase comparisons, a factor $2kR$ was subtracted from the total XAFS phase in Eq. (1). The experimental energy reference E_0 was chosen by comparing the total absorption curve of experiment with near edge band-structure calculations,[19] and no shifts in E_0 were allowed [see Fig. 6(a)].[29] To avoid ambiguity, both calculated and experimental XAFS were filtered in an identical manner, with a filtering window $1.68 < R < 2.79$ Å and a Hanning function on the edges of width 0.2 Å.

As seen from Fig. 2 self-consistency is only important for $k < 3$ Å^{-1} (i.e., within about 30 eV of threshold) with all calculated curves giving similar results in the high-energy region. The finding that self-consistency is generally unnecessary for *ab initio* XAFS calculations permits an important simplification. Although self-consistent potentials may be needed at lower energies, the differences with experiment observed in Fig. 2 for $k > 3$ Å^{-1} cannot be eliminated by better prescriptions for V_C. This discrepancy indicates that the errors incurred by the use of ground-state self-energies calculations can be as large as those due to the PWA and hence that excited-state self-energies and other many-body corrections are *essential* in XAFS calculations.

B. Self-energy in XAFS

The use of an excited-state self-energy in the scattering potential for XAFS calculations was first discussed by Beni, Lee, and Platzman.[36] Subsequently Lee and Beni[2] found that the *GW* plasmon-pole self-energy of Hedin and Lundqvist[20,21] can give good agreement between theoretical and experimental XAFS phases. However, this comparison was done in the context of plane-wave calculations, using E_0 and S_0^2 as fitting parameters. Others have found that a Dirac-Hara form[22] for the self-energy can also lead to good agreement.[37] To assess the accuracy of these self-energies more precisely, it is therefore necessary to perform comparisons with experiment using both a correct curved-wave formulation and an unambiguous energy reference. To this end we have examined the effect of several self-energy prescriptions on XAFS phases and amplitudes: namely the HL (Refs. 20 and 21) and DH (Ref. 22) energy-dependent self-energies as well as the ground-state Slater[16] X_α and von Barth–Hedin[17] V_{xc}.

To compare calculated amplitudes with experiment, it is necessary to account for inelastic losses.[8] These include inelastic losses associated with the relaxation of the core hole (intrinsic processes), inelastic losses suffered by the photoelectron (extrinsic processes), and interference between these two processes. The intrinsic processes are included in the passive electron overlap factor S_0^2 and in the core-hole lifetime, while the extrinsic processes are contained in the imaginary part of the self-energy. In Ref. 12 it was found that the effect of the interference between extrinsic and intrinsic losses was an approximate cancellation of the passive electron overlap factor S_0^2 and the imaginary part of the dynamical correction to the central-atom phase shift in the outgoing path of the photoelectron δ_{out}^c, i.e.,

$$S_0^2(E)\exp[-(\mathrm{Im}\delta_{out}^{dyn})] \cong 1 .$$

Thus we have simply approximated $S_0^2 = \text{const} \cong 1$ and neglected dynamical interference effects. Ground-state V_{xc} and the DH self-energy are real and thus do not include extrinsic losses; for these potentials a mean free path term is introduced using a constant imaginary potential. In contrast, the complex HL self-energy automatically includes extrinsic losses. Heretofore, the calculation of the HL self-energy was the computational bottleneck in XAFS calculations, as the simplest representation consists of one-dimensional integrals. Tabulations are also available,[38] but they do not cover the range of energies and densities necessary for XAFS calculations. To circumvent this difficulty, we have introduced a fast, analytic approximation to the HL self-energy as discussed in the Appendix.

In Fig. 3, we compare the XAFS phase calculated using the above self-energies with Cu K-edge experimental data.[32] Both experimental and calculated XAFS were filtered in the same way as the results of Fig. 2, i.e., with a filtering window $1.68 < R < 2.79$ Å and Hanning function edges of width 0.2 Å. The calculation with the HL potential is observed to have the best agreement with experiment, with an error in phase less than 0.2 rad even at $k = 2.5$ Å^{-1}. The increased deviation at $k > 14$ Å^{-1} is likely due to the error in the near-neighbor distance and to experimental noise. The calculations using ground-state potentials have differences with experiment of at least 1 rad. The curve representing the DH calculation can be brought to a closer agreement with experiment in the range $4 < k < 12$ Å^{-1} if a shift of -9 eV is applied to the experimental data. However, the maximum energy shift consistent with the uncertainty in E_0 in our calcula-

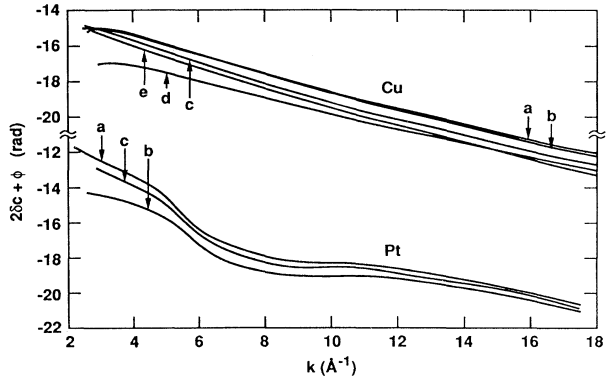

FIG. 3. Filtered XAFS phase ($2\delta^c + \Phi$) for the first coordination shell of Cu (K edge) calculated with various exchange-correlation potentials and self-energies: (a) $X\alpha$ potential, (b) von Barth–Hedin potential, (c) HL self-energy, (d) DH self-energy, and (e) experiment; similarly for the first coordination shell of Pt (L_{III} edge): (a) HL self-energy, (b) DH self-energy, and (c) experiment.

tion is less than 4 eV. The discrepancy between experiment and the HL result has two likely origins: an error in our estimate of the Fermi level (about 4 eV in our calculation) and an inadequacy of the HL self-energy itself.[39] We found similar trends in other cases (Ge, Br_2, Pt), i.e., the experimental phase is usually closer to the HL result but lies between the HL and DH curves.[29] The result for the XAFS phase in Pt at 190 K is also shown in Fig. 3. In this case we set $R=2.778$ Å and the energy reference E_0 was chosen as the peak of the white-line in the absorption spectrum. As band-structure calculations of x-ray absorption were not available for Pt, this choice was based on calculations for Pd, which has a similar valence electronic configuration.[40] In these comparisons, experimental and theoretical XAFS were filtered over the ranges $2.5 \leq k \leq 18$ Å^{-1} and $1.5 \leq R \leq 2.5$ Å.

A comparison of XAFS amplitudes is shown in Fig. 4. It should be noted that the falloff of the total atomic absorption coefficient μ_0 will introduce a correction in the experimental XAFS, defined using edge-step normalization as

$$\chi(E)=[\mu(E)-\mu_0(E)]/\Delta\mu_0(E_0)$$

of about 10–20% at high k;[32] however, this correction was not included in Fig. 4. In this comparison we used the atomic value $S_0^2=0.7$, given in Refs. 31 and 32. From Fig. 4 it is apparent that the curve computed with the HL self-energy is again closest to experiment. This is mainly due to the neglect of extrinsic losses in the other self-energies, but also indicates that the HL potential gives a good approximation to the extrinsic losses. We also observe that $S_0^2=0.7$ is too small; in the next section (see Table I) it is shown that values $0.85 \leq S_0^2 \leq 1.1$, lead to reasonable agreement between theoretical (using the HL self-energy) and experimental XAFS amplitudes.

We conclude that ground-state exchange-correlation potentials lead to XAFS phase errors as large as those introduced by the PWA. The HL self-energy yields better agreement with experiment than the DH self-energy, but the experimental phase typically lies in between. A study of possible corrections to the plasmon-pole HL self-energy is currently underway.[41]

C. Energy scaling in x-ray-absorption calculations

As pointed out above, the HL self-energy leads to reasonable agreement between calculated and experimental XAFS phases and amplitudes. We also found that calculations of the XAFS phase using ground-state V_{xc} do not agree with those results even when a shift of E_0 is added.[29] However, Materlik, Muller, and Wilkins observed[40] that band-structure calculations of x-ray absorption using ground-state V_{xc} could be brought into reasonable agreement with experiment in the energy range 0–100 eV simply by rescaling the theoretical energy axis as $E \rightarrow E'=\alpha E$, where $1.04<\alpha<1.07$. In particular they found $\alpha=1.05$ for L_{III} absorption in Gd.[40] We offer below an alternative explanation of this observation.

In Fig. 5 we plot the quantity $E'=E+\Delta(E)$ for Gd in the energy range 0–8 Ry (0–108 eV). Here

$$\Delta(E)=\mathrm{Re}[\Sigma(E,\rho_{\mathrm{int}})-\Sigma(\mu,\rho_{\mathrm{int}})] ,$$

where $\Sigma(\mu,\rho_{\mathrm{int}})$ is the self-energy contribution to the muffin-tin potential at threshold, $E=\mu$. For the case in which a HL self-energy is used, we found $E'=E+\Delta(E)$ can be approximated as a straight line, $E' \cong 1.05E$, which is in accord with the result of Ref. 40. We also found that the DH self-energy yields $E'=E+\Delta(E) \cong 1.101E$, which is inconsistent with the observed scaling.

The observed scaling can thus be understood simply as a consequence of the energy dependence of the muffin-tin zero, i.e., as the energy dependence arising from the slow turning off of the exchange-correlation hole with increasing energy. Evidently the linear form of rescaling is only valid at low energies. Our explanation also suggests a simple but reasonably accurate way to correct XAFS calculations that use ground-state correlation potentials, without the need for linearization. One simply redefines the energy scale to be $E \rightarrow E'=E+\Delta(E)$, with $\Delta(E)$ cal-

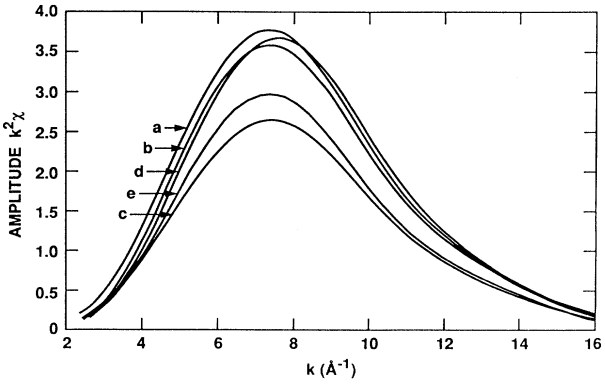

FIG. 4. Filtered total XAFS amplitude of $k^2\chi(k)$ for the first coordination shell of Cu (K edge) calculated with various exchange-correlation potentials and self-energies: (a) $X\alpha$ potential, (b) von Barth–Hedin potential, (c) HL self-energy, (d) DH self-energy, and (e) experiment.

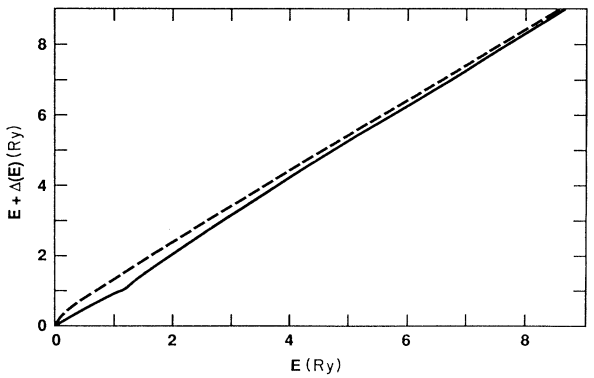

FIG. 5. Energy rescaling $E'=E+\Delta(E)$ in Gd, where $\Delta E=\mathrm{Re}[\Sigma(E,\rho_{\mathrm{int}})-\Sigma(\mu,\rho_{\mathrm{int}})]$, using the HL self-energy (solid line, $E' \cong 1.05E$) and using the DH self-energy (dashed line, $E' \cong 1.001E$).

culated using the HL self-energy. This requires the evaluation of the self-energy only at the interstitial density. Moreover, the amplitude can also be corrected approximately by using a Lorentzian broadening that includes the imaginary part of the self-energy, i.e., with a width

$$\Gamma'(E)=\Gamma-2\,\mathrm{Im}\Sigma(E,\rho_{\mathrm{int}})\ ,$$

where Γ is the full linewidth associated with the core-hole lifetime.

IV. *Ab initio* XAFS CODE FEFF

With the approximations determined in the above studies, we have developed an automated code for efficient, *ab initio* curved-wave XAFS calculations. The complete code is termed FEFF for the role of the effective, curved-wave scattering amplitude in the theory. The code is arranged in primary subroutines that correspond to the main steps in the calculation of XAFS: (i) calculation of atomic potentials and densities, (ii) generation of a muffin-tin scattering potential that includes the excited-state self-energy and calculated energy reference, (iii) calculation of complex partial wave-scattering phase shifts, and (iv) the calculation of curved-wave-scattering amplitudes and phase shifts, together with the exact, single-scattering curved-wave XAFS spectra.

A summary of the ingredients in the code follows; for additional detail see the foregoing discussion and Ref. 13. Our atomic potentials and charge densities are based on the relativistic Dirac-Fock-Slater atom code of Desclaux,[14] which we have automated for all atoms through americium ($Z=95$). This relativistic code is a notable improvement over the tabulated Clementi-Roetti Hartree-Fock atomic wave functions of Ref. 3 or the nonrelativistic $X\alpha$-based Herman-Skillman wave functions of Ref. 4. Our scattering potential is based on the overlapping atom prescription of Mattheiss together with an automated Norman prescription for calculating the muffin-tin radii.[33,34]

This scattering potential also includes a complex, energy- and density-dependent self-energy, $\Sigma(E,\rho)$, which leads to significant improvements in the XAFS phase compared with ground-state V_{xc}.[13,29] Our self-energy is based on the GW formulation of Hedin and Lundqvist[20] with the plasmon-pole approximation for the electron-gas dielectric function. This is the same self-energy as introduced by Lee and Beni[2] and incorporated into the tables of Teo and Lee.[3] However, their implementation is computationally time consuming; indeed the main reason that improved self-energies have not been used more generally is their difficulty of calculation. To circumvent this difficulty, we have introduced a fast, analytic approximation for the real part and an exact expression for the imaginary part, as discussed in the Appendix. The efficiency of our code is due largely to this improvement. Note that because the self-energy is energy dependent, the muffin-tin zero of the scattering potential is also energy dependent. This implies that the concept of the "inner potential," which is often invoked in XAFS analysis, is ambiguous. To circumvent this ambiguity, we have chosen the photoabsorption energy threshold (i.e., the Fermi level in a metallic solid) as the fixed-energy reference E_0. From this reference the photoelectron wave number is defined as $k=\sqrt{2(E-E_0)}$ in atomic units, i.e., k in inverse Bohr and E in hartrees. In the code, the value of E_0 is estimated from electron-gas theory, based on the average interstitial electron density. Finally, single-scattering contributions to XAFS are calculated using the exact curved-wave formulation based on effective scattering amplitudes,[1] yielding χ in the standard form of Eq. (1). We stress that the quantity $f_{\mathrm{eff}}(\pi,k,R)$ in Eq. (1), which is defined with respect to a well-defined photoelectron wave number $k=\sqrt{2(E-E_0)}$ for comparison with experiments, is not the same as the curved-wave scattering amplitude $\tilde{f}(\pi,p,R)$ of other treatments.[4,6,10] The relation between these is

$$f_{\mathrm{eff}}=(k/p)\exp[i2(\mathrm{Re}p-k)R]\tilde{f}\ ,$$

where the (complex) photoelectron momentum p defined with respect to the complex interstitial potential $V_{\mathrm{int}}(E)$ is given by

$$p=\sqrt{2[E+i\Gamma/2-V_{\mathrm{int}}(E)]}\ ,$$

and Γ is the full linewidth of the core-hole state.

Besides χ_l as a function of k, FEFF yields all of the amplitudes and phases appearing in Eq. (1), thus removing the "black-box" aspect of *ab initio* codes. Thus these amplitudes and phases may be used in experimental fits the same way as present XAFS tables are. More precisely, the factor $\exp(2ipR)/pR^2$ in Eq. (4) is replaced by $\exp(2ikR)/kR^2$, and $\tilde{f}$ is replaced by f_{eff}. Therefore we give as output $|f_{\mathrm{eff}}(\pi,k,R)|$, $\Phi_{\mathrm{eff}}(\pi,k,R)$; $\mathrm{Re}\delta^c$, $s_0^2=S_0^2\exp(-2\,\mathrm{Im}\delta^c)$, and $\lambda=1/\mathrm{Im}p$ all tabulated as a function of k. The code also has a provision for a Debye-Waller factor $e^{-2\sigma^2k^2}$ and an additional reduction factor S_0^2, which may be determined from known values or simply used as fitting parameters.[31,42]

An added advantage of the FEFF code over tables of XAFS amplitudes and phases is the flexibility of altering atomic and structural parameters to simulate the chemical environment around an absorbing atom, rather than simply assuming identical, independent atoms and depending on the hypothesis of chemical transferability. Furthermore, the efficiency of FEFF makes possible *ab initio* calculations of XAFS even on workstations or many personal computers. Thus, these *ab initio* standards can be used as routinely as current tables. For example, the total CPU time on a Digital Equipment Corporation VAX 3100 workstation is about 3.5 min for 400 energy points between $0<k<20$ Å^{-1}.

V. COMPARISON WITH EXPERIMENT

In this section we present comparisons between XAFS spectra generated using the *ab initio* code FEFF, as discussed in Sec. IV, and experiment in a number of test cases, namely, Cu, Ge, Pt, Br_2, and $GeCl_4$. The first shell contributions to the experimental data were isolated using the following filtering windows: $1.68\le R\le 2.69$ Å for Cu, $1.70\le R\le 2.50$ Å for Ge, $1.80\le R\le 2.93$ Å for

TABLE I. Input parameters in XAFS calculations and estimated errors with respect to experiment: N is the coordination number of the absorbing atom, R the nearest-neighbor distance, σ^2 the mean-square vibrational amplitude, $\delta\sigma^2$ the "McMaster correction" (Ref. 43) (see text), ΔR and $\Delta\sigma^2$ discrepancies between theoretical and experimental values, S_0^2 an overall amplitude factor needed to fit experiment, and E_0 the position of our calculated energy reference.

Compound, edge	N	R (Å)	σ^2 (Å^2)	$\delta\sigma^2$ (Å^2)	ΔR (Å)	$\Delta\sigma^2$ (Å^2)	S_0^2	E_0 (eV)
Cu K (190 K)	12	2.552[44]	0.005 30[32]	0.000 58	0.017 8	0.000 19	0.845	8 982
Pt L_{III} (190 K)	12	2.771 5[44]	0.003 21[32]	0.000 40	0.002 3	0.000 45	0.893	11 568
Ge K (300 K)	4	2.450[44]	0.003 59[2]	0.000 32	0.001 1	0.000 08	1.09	11 088
$GeCl_4$Ge K (300 K)	4	2.110[45]	0.002 12[46]	0.000 32	0.002 9	0.001 53	1.11	11 082
Br_2 K (300 K)	1	2.280[8]	0.001 98[8]	0.000 32	0.005 6	0.000 45	1.08	13 456

Pt, $1.73 \leq R \leq 2.22$ Å for Br_2, and $1.00 \leq R \leq 2.00$ Å for $GeCl_4$. Hanning functions of width 0.2 Å were used at the edges of all filtering windows. The filtering range in k space is shown in Fig. 7. To avoid ambiguities the calculated XAFS were filtered in identical manner. The structural parameters are given in Table I. The quality of agreement between theory and experiment was then quantified by (i) the discrepancy between the observed nearest-neighbor distance from experiment and the crystallographic value used in the calculations (ΔR in Table I), (ii) the discrepancy between the Debye-Waller factor from the fit and the known values ($\Delta\sigma$ in Table I), and (iii) the value of the reduction factor S_0^2 needed to fit experimental amplitudes. The values of E_0 were chosen to correspond to near-edge absorption data and are shown in Fig. 6 and listed in Table I. Also the calculated XAFS were modified to correct for the edge-step normalization of the experimental spectra[32,44–46] by introducing a small positive "McMaster correction,"[43] $\delta\sigma^2$, to the Debye-Waller factor, as listed in Table I.

As seen in Fig. 7 the overall agreement between theory and experiment is very good in all cases. From Table I,

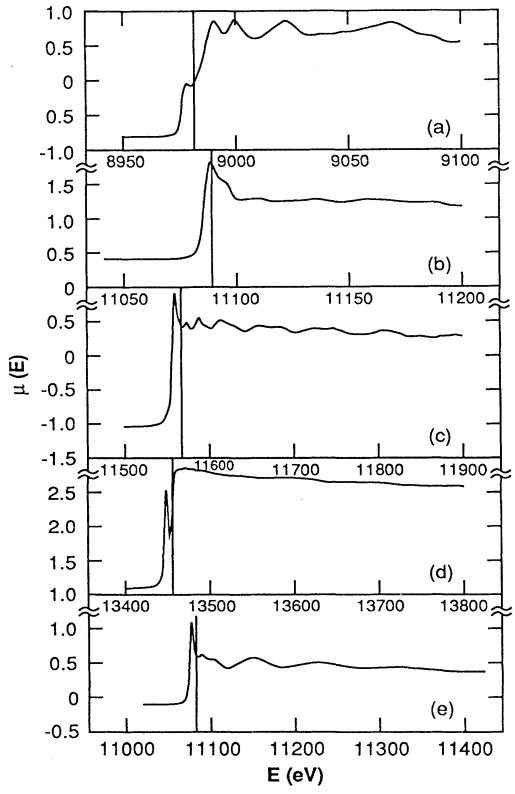

FIG. 6. Measured x-ray-absorption coefficient $\mu(E)$ for (a) Cu K edge at 190 K, (b) Ge K edge at 300 K, (c) Pt L_{III} edge at 190 K, (d) $GeCl_4$ K edge at 300 K, and (e) Br_2 K edge at 300 K. The vertical lines indicate the position of the energy reference E_0 corresponding to our calculation.

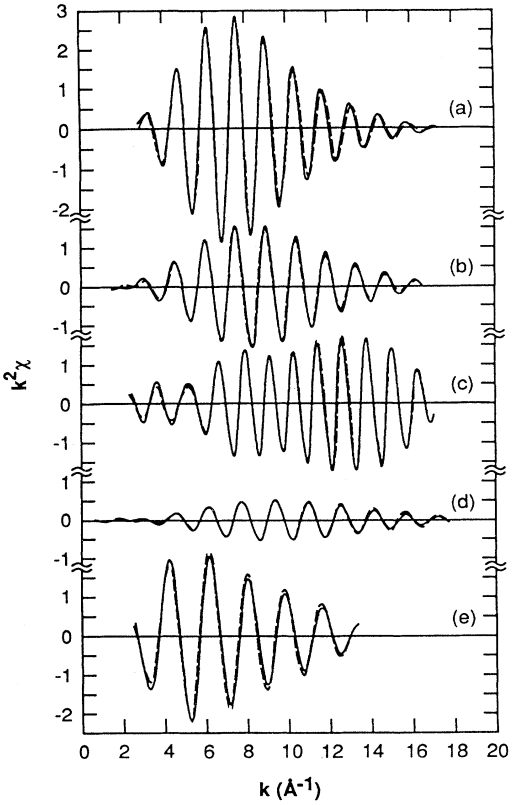

FIG. 7. Filtered XAFS $k^2\chi(k)$ calculated (solid line) and measured (dashed line) for the first coordination shell of (a) Cu K edge at 190 K, (b) Ge K edge at 300 K, (c) Pt L_{III} edge at 190 K, (d) $GeCl_4$ K edge at 300 K, and (e) Br_2 K edge at 300 K.

the accuracy in the nearest-neighbor distance determination is always better than 0.02 Å, and the discrepancy in the Debye-Waller factor is better than 0.0015 Å^2. Values of the amplitude reduction factor indicate that the use of FEFF with $S_0^2 \cong 0.9$ leads to uncertainties in the determination of nearest-neighbor coordination numbers smaller than 15%.

VI. SUMMARY AND CONCLUSIONS

We have elucidated what we believe are the most important factors needed for quantitative calculations of XAFS. Curved-wave effects and relativistic potentials are well known to be important. In addition, from comparisons of theoretical and experimental XAFS phases, we find that it is essential to use an energy-dependent complex self-energy to account for inelastic losses and self-energy shifts. We find that the HL self-energy leads to phases that agree better with experiment than those calculated with the DH potential. However, the experimental phase is usually slightly shifted from the Hedin-Lundqvist result in the direction of the DH result, indicating the need to explore possible corrections to the self-energy.[39,41] A good overlapped-atom potential and a fixed-energy reference are next in importance. We have found that an automated prescription based on the Norman prescription for determining muffin-tin radii can give results for XAFS comparable to those obtained with self-consistent potentials, except very close to the absorption edge. The use of the HL self-energy can also explain the empirical energy scalings[40] observed in band-structure calculations of x-ray-absorption spectra, without the need for more elaborate explanations. The HL self-energy at the interstitial density also provides a simple prescription for correcting XAFS calculations that used a ground-state V_{xc}.

Based on our findings, we have developed an automated code FEFF to calculate single-scattering XAFS. The code takes into account all of the important features outlined above, including spherical wave corrections, overlapping relativistic-atom scattering potentials, an excited-state self-energy, and an unambiguous energy reference, and is fast enough to be used in routine experimental analysis in much the same way as current tabulations. The XAFS phases obtained agree with experiment to better than 0.1 rad, even at energies as low a 10 eV from the absorption edge. Nearest-neighbor distances are predicted with errors less than 0.02 Å. Amplitudes are predicted with an accuracy of 15%, leading to the same accuracy in coordination number determination. The error in the energy origin $E_0 \cong 4$ eV is attributed to errors in the construction of the scattering potential and in our estimate of the chemical potential; however, this effect appears to be less important than the need for an energy-dependent self-energy.

In order to achieve better accuracy in the XAFS phase close to threshold, it may be necessary to use better scattering potentials and self-energies at low energies and also to improve our estimate of E_0. To improve the accuracy of the XAFS amplitude it is probably necessary to calculate the energy dependence of the amplitude reduction factor $S_0^2(E)$, including dynamical corrections to the inelastic losses. Efforts along these lines are in progress.

ACKNOWLEDGMENTS

We wish to thank E. A. Stern, C. Bouldin, and H. Kim for providing experimental data, A. Djaoui for assistance in coding the complex phase shifts, and other colleagues, especially S. Cramer, D. Lu, C. R. Natoli, R. Felton, E. A. Stern, T. Tyson, and D. Sayers for valuable comments and suggestions. We especially thank the National Synchrotron Light Source (NSLS) and the X-11 PRT at Brookhaven National Laboratory for hospitality and support in the development of a preliminary version of the automated code FEFF. This work was supported in part by the U.S. Department of Energy (DOE) through Grant No. DE-FG06-90ER45415 (J.J.R.) and through the Center for Materials Science at Los Alamos National Laboratory (J.M and R.C.A.).

APPENDIX: HEDIN-LUNDQVIST SELF-ENERGY APPROXIMATION

As shown by Lundqvist,[21] the electron-gas self-energy in the GW–plasmon-pole approximation of Hedin and Lundqvist, can be expressed as a sum of one-dimensional integrals, which depend on the quasiparticle energy $E=p^2/2$ and momentum p. For an atom (where the electron density is nonuniform) p is taken to be the density-dependent local momentum, i.e., $p \rightarrow p(\mathbf{r})=[2E+k_F^2(\rho(\mathbf{r}))]^{1/2}$. Evaluating the numerical integrals for every energy and local momentum $p(\mathbf{r})$ leads to a computational bottleneck. To avoid this difficulty, we fit the real part of Σ to a three-term polynomial in $r_s^{1/2}$,

$$\frac{\mathrm{Re}\Sigma}{E_F} = a_1(x) r_s + a_2(x) r_s^{3/2} + a_3(x) r_s^2 , \tag{A1}$$

where $r_s=(3/4\pi\rho)^{1/3}$ is the density parameter, $x=p/k_F$, and $E_F=k_F^2/2$ is the Fermi energy. We then fit the coefficients $a_n(x)$ to polynomials in x or $1/x$, i.e.,

$$a_n(x) = \begin{cases} d_0^n + d_1^n x + d_2^n x^2 + d_3^n x^3, & x \le x_c \\ (c_1^n/x) + (c_2^n/x^2), & x > x_c \end{cases} . \tag{A2}$$

The point x_c corresponds to the value at which the real part of Σ exhibits a cusplike dip (Fig. 8), and is the onset of the imaginary part. It is determined by the threshold for plasmon emission: $\epsilon_{p+q}=\omega_q+\epsilon_p$, where ϵ_{p+q} is the energy of the initial electron, ω_q is the plasmon energy ($\hbar=1$), and ϵ_p is the electron final energy. Numerically this corresponds to the real solution of the equation $\omega^2(q)=(x^2-1)^2$, where $\omega(q)$ is the plasmon dispersion relation,[20]

$$\omega^2(x) = \omega_p^2 + E_F^2(\tfrac{4}{3}x^2 + x^4) , \tag{A3}$$

where $\omega_p=(4\pi\rho)^{1/2}$ is the plasma frequency. The electron density in an atom varies from metallic densities in the outer part $r_s \sim 4$ to $r_s \sim 0.001$ in the core region. To fit this entire range, we found it useful to make four partitions covering successive density regimes: $0<r_s<0.2$, $0.2<r_s<1.0$, $1.0<r_s<5.0$, and $r_s>5.0$.

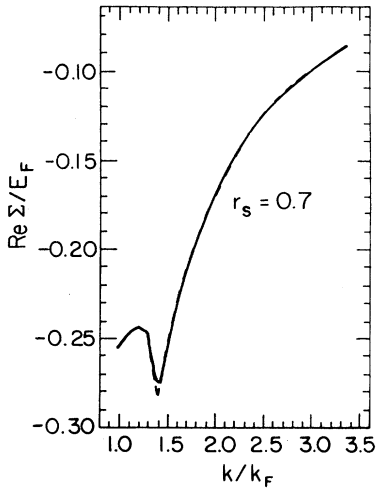

FIG. 8. Real part of the HL self-energy (divided by E_F) for a free-electron gas with density parameter $r_s=0.7$. Numerical calculation (solid line) and analytic fit from Eq. (A1) (dashed line).

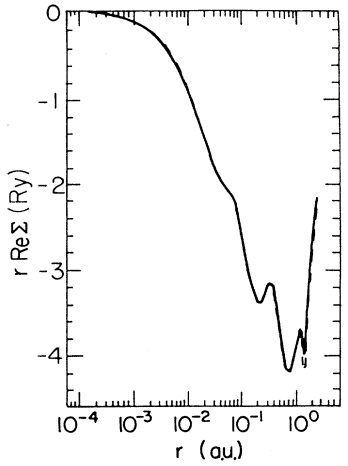

FIG. 9. Real part of the HL self-energy times r in atomic units, for a photoelectron with energy $E-\mu=16$ Ry, in a Ni atom. Numerical calculation (solid line) and analytic fit from Eq. (A1) (dashed line).

For the imaginary part, we have shown that the integrals can all be evaluated analytically, yielding for $p>k_F$,

$$\frac{\mathrm{Im}\Sigma}{E_F}=\Theta_+(x)[f(q_+)-f(1+x)]+\Theta_u(x)[f(q_u)-f(x-1)]+\Theta_-(x)[f(x-1)-f(q_-)]\ . \tag{A4}$$

Here

$$\Theta_+(x)=\Theta(q_+-(1-x))\ ,$$

$$\Theta_u=\Theta(q_u-(x-1))\ ,$$

$$\Theta_-(x)=\Theta((x-1)-q_-)\ ,$$

where

$$\Theta(x)=\{1(x>0)\text{ or }0(x<0)\}$$

is the unit-step function,

$$q_u(x)=\min\{q_3(x),1+x\}$$

where q_3/k_F is the positive solution of the quadratic equation $\omega^2(x)=(x^2-1)^2$, $q_\pm(x)$ are the positive roots of the cubic equation $\omega_p^2+(\frac{4}{3}-4x^2)q^2+4xq^3=0$, and the function

$$f(x)=(\omega_p/4k_Fx)\ln\{[\omega(x)+\omega_p]/x^2+\tfrac{2}{3}\omega_p\}\ .$$

In Figs. 8 and 9 we compare the self-energy obtained from the fit with the numerical integral expression for the self-energy for both a homogeneous electron gas and for atomic Ni. We find that the XAFS scattering phase shifts and the backscattering amplitude calculated numerically or with our fit agree to better than 1%.

Having devised an efficient method to generate the Hedin-Lundqvist self-energy, we need to ensure that the excited-state self-energy $\Sigma(p,E)$ will reduce to the correct ground-state self-energy potential in the limit $E\to\mu$, where μ is the chemical potential. To this end we have followed the prescription introduced by Wang and Pickett[47]

$$\Sigma(p,E)=V_{\mathrm{xc}}(\rho)+\Sigma_{\mathrm{HL}}(p,E,\rho)-\Sigma_{\mathrm{HL}}(k_F,\mu,\rho)=V_{\mathrm{xc}}(\rho)+\Delta(p,E,\rho)\ , \tag{A5}$$

Here, $\Sigma_{\mathrm{HL}}(p,E,\rho)=\Sigma^0_{\mathrm{HL}}(p,E-\mu+E_F)$ is the HL self-energy and $V_{\mathrm{xc}}(\rho)$ is the ground-state exchange-correlation potential. Thus we compute Δ using

$$\Delta(p,E,\rho)=\Sigma^0_{\mathrm{HL}}(p,E-\mu+E_F,\rho)-\Sigma^0_{\mathrm{HL}}(k_F,k_F^2/2,\rho)\ . \tag{A6}$$

The local momentum p is obtained using the local density equations, that give[2]

$$p^2=k_F^2+2(E-\mu)+2\Delta(p,E-\mu)\ . \tag{A7}$$

In Ref. 2 the contribution 2Δ in Eq. (A7) is ignored. We evaluate Eqs. (A6) and (A7) using two iterations: First we evaluate Eq. (A6) using $p^2=k_F^2+2(E-\mu)$. This yields a value for Δ, which is used in Eq. (A7), leading to a new value of p, which is inserted in Eq. (A6); we then evaluate $\Sigma(p,E)$ using Eq. (A5). This approach leads to a small correction of 0.8 eV (in Cu) in the value of the self-energy at $E=\mu$, and avoids a discontinuity at threshold. The same approach is used for the DH self-energy.

*Present address: Exploratory Development and Electronics Research Group, Los Alamos National Laboratory, Los Alamos, New Mexico 87545.

[1]J. J. Rehr, R. C. Albers, C. R. Natoli, and E. A. Stern, Phys. Rev. B **34**, 4350 (1986).

[2]P. A. Lee and G. Beni, Phys. Rev. B **15**, 2862 (1977).

[3]B. Teo and P. A. Lee, J. Am. Chem. Soc. **101**, 2815 (1979).

[4]A. G. McKale, B. W. Veal, A. P. Paulikas, S.-K. Chan, and G. S. Knapp, J. Amer. Chem. Soc. **110**, 3763 (1988).

[5]P. A. Lee and J. B. Pendry, Phys. Rev. B **11**, 2795 (1975).

[6]A. G. McKale, G. S. Knapp, and S.-K. Chan, Phys. Rev. B **33**, 841 (1986).

[7]P. J. Durham, J. B. Pendry, and C. H. Hodges, Comput. Phys. Commun. **25**, 193 (1982).

[8]S. H. Chou, J. J. Rehr, E. A. Stern, and E. R. Davidson, Phys. Rev. B **35**, 2604 (1987); J. J. Rehr, E. A. Stern, R. L. Martin, and E. R. Davidson, *ibid.* **17**, 560 (1978).

[9]S. J. Gurman, J. Phys. C **21**, 3699 (1988).

[10]W. Schaich, Phys. Rev. B **29**, 6513 (1984).

[11]P. A. Lee, Phys. Rev. B **13**, 5261 (1976).

[12]D. Lu and J. J. Rehr, Phys. Rev. B **37**, 6126 (1988); W. Ekardt and D. B. Tran Thoai, Solid State Commun. **40**, 939 (1981); L. Hedin, Physica B **158**, 344 (1989).

[13]J. J. Rehr, J. Mustre de Leon, S. Zabinsky, and R. C. Albers, J. Amer. Chem. Soc. **113**, 5135 (1991).

[14]J. Desclaux, J. Phys. B **4**, 631 (1971); J. Desclaux, Comput. Phys. Commun. **9**, 31 (1975).

[15]L. J. Sham and W. Kohn, Phys. Rev. **145**, 561 (1966).

[16]J. Slater, Phys. Rev. **81**, 385 (1951).

[17]U. von Barth and L. Hedin, J. Phys. C **5**, 1629 (1972).

[18]C. R. Natoli, M. Benfatto, T. A. Tyson, K. O. Hodgson, and B. Hedman (unpublished).

[19]R. C. Albers, A. K. McMahan, and J. E. Müller, Phys. Rev. B **31**, 3435 (1985); A. K. McMahan and R. C. Albers, Phys. Rev. Lett. **49**, 1198 (1982).

[20]L. Hedin and S. Lundqvist, Solid State Phys. **23**, 1 (1969).

[21]B. I. Lundqvist, Phys. Kondens. Mater. **6**, 206 (1977).

[22]P. A. M. Dirac, Proc. Cambridge Philos. Soc. **26**, 376 (1930).

[23]J. E. Müller and J. W. Wilkins, Phys. Rev. B **29**, 4331 (1984).

[24]P. A. Lee, P. H. Citrin, and B. M. Kincaid, Rev. Mod. Phys. **53**, 769 (1980).

[25]J. J. Barton and D. A. Shirley, Phys. Rev. B **32**, 1892 (1985); J. Muller and W. Schaich, *ibid.* **27**, 6489 (1983).

[26]J. Mustre de Leon, J. J. Rehr, C. R. Natoli, C. S. Fadley, and J. Osterwalder, Phys. Rev. B **39**, 5632 (1989).

[27]M. Benfatto, C. R. Natoli, C. Brouder, R. F. Pettifer, and M. F. Ruiz López, Phys. Rev. B **39**, 1936 (1989).

[28]D. B. Tran Thoai and W. Ekardt, Solid State Commun. **40**, 264 (1981).

[29]J. Mustre de Leon, Ph.D. thesis, University of Washington, 1989.

[30]K. Rahkonen and K. Krause, At. Data Nucl. Data Tables **14-2**, 140 (1974).

[31]T. A. Carlson, *Photoelectron and Auger Spectroscopy* (Plenum, New York, 1975).

[32]E. A. Stern, B. A. Bunker, and S. M. Heald, Phys. Rev. B **21**, 5521 (1980).

[33]L. Mattheiss, Phys. Rev. **133**, A1399 (1964).

[34]J. G. Norman, J. Mol. Phys. **31**, 1191 (1976).

[35]T. L. Loucks, *Augmented Plane-Wave Method* (Benjamin, New York, 1967).

[36]G. Beni, P. A. Lee, and P. M. Platzman, Phys. Rev. B **13**, 5170 (1976).

[37]P. Sainctavit, J. Petiau, M. Benfatto, and C. R. Natoli, in *Proceedings of the Fifth International Conference on X-Ray Absorption Fine Structure,* edited by J. Mustre de Leon *et al.* (North-Holland, Amsterdam, 1989).

[38]L. Hedin and B. I. Lundqvist, J. Phys. C **4**, 2064 (1971).

[39]P. Horsch, W. von der Linden, and W. D. Lukas, Solid State Commun. **62**, 359 (1987).

[40]G. Materlik, J. E. Muller, and J. W. Wilkins, Phys. Rev. Lett. **50**, 267 (1983); J. W. Wilkins, in *X-Ray and Atomic Inner Shell Physics,* edited by B. Crasemann (AIP, New York, 1982), p. 687.

[41]J. J. Rehr *et al.*, Bull. Am. Phys. Soc. **140**, 776 (1990).

[42]E. Sevillano, H. Meuth, and J. J. Rehr, Phys. Rev. B **20**, 4908 (1979).

[43]W. H. McMaster, N. Kerr–Del Grande, J. H. Mallet, and J. H. Hubbell (unpublished).

[44]W. G. Wickoff, *Crystal Structures,* 4th ed. (Interscience, New York, 1974). Nearest-neighbor distances are given at 18 °C, and then corrected using thermal expansion data from *American Institute of Physics Handbook* (McGraw-Hill, New York, 1963).

[45]C. E. Bouldin, G. Bunker, D. A. McKeown, R. A. Forman, and J. J. Ritter, Phys. Rev. B **38**, 10 816 (1988).

[46]Y. Marino, Y. Nakamura, and T. Iijima, J. Chem. Phys. **32**, 643 (1960).

[47]C. S. Wang and W. E. Pickett, Phys. Rev. Lett. **51**, 597 (1983); W. E. Pickett and C. S. Wang, Phys. Rev. B **30**, 4719 (1984).